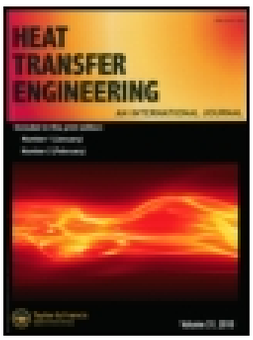

Heat Transfer Engineering

ISSN: 0145-7632 (Print) 1521-0537 (Online) Journal homepage: http://tandfonline.com/loi/uhte20

# Feasibility of Computational Fluid Dynamics for Analyzing Airflow around Porous Fences

Yizhong Xu, Rajnish K. Calay & Mohamad Y. Mustafa

**To cite this article:** Yizhong Xu, Rajnish K. Calay & Mohamad Y. Mustafa (2018): Feasibility of Computational Fluid Dynamics for Analyzing Airflow around Porous Fences, Heat Transfer Engineering, DOI: 10.1080/01457632.2018.1546663

**To link to this article:** https://doi.org/10.1080/01457632.2018.1546663

Accepted author version posted online: 21 Dec 2018.

# FEASIBILITY OF COMPUTATIONAL FLUID DYNAMICS FOR ANALYZING AIRFLOW AROUND POROUS FENCES

**Yizhong Xu, Rajnish K. Calay and Mohamad Y. Mustafa**

Department of Building, Energy and Material Technology, UiT/ the Arctic University of Norway, Narvik, Norway

Address correspondence to Dr. Yizhong Xu, Department of Building, Energy and Material Technology, UiT/ the Arctic University of Norway, Lodve Langes gt. 2, Postboks 385, 8505, Narvik, Norway. E-mail: Yizhong.Xu@uit.no

Phone Number: +47 76 96 65 44, Fax Number: +47 76 96 68 10



***ABSTRACT***

*This paper presents using the computational fluid dynamics (CFD) modelling to analyze the flow around porous fences. The feasibility of applying two- and three-dimensional models was assessed with respect to corresponding wind tunnel experiments. Comparisons between the flow structures on leeward of the fence as predicted by CFD models and the wind tunnel measurements were discussed. Velocity values for the two modelling approaches were in good agreement. However, there is a noticeable discrepancy in predicting the turbulence structure. Both two- and three-dimensional model have demonstrated the capability to predict flow characteristics necessary for the design of porous fences. However, the selection between two- and three-dimensional model is dependent on, design stage and the extent of accuracy required by the application. The*

*presented CFD models are potentially applicable to heat transfer issues.*

## *INTRODUCTION*

Windbreaks are found in many areas and applications. Natural windbreaks such as natural foliage, tall hedgerows, and tree lines can create low velocity by blocking or retarding ground level winds and diverting higher winds over the area to be shielded. When natural windbreaks are not available or not appropriate, particularly in built or extremely harsh climatic environments, artificial means of achieving the effect of windbreaks are required, leading to the design and construction of porous fences. Porous fence is one of common devices used to improve windy and snowy climatic conditions to serve human needs. It has been widely used in coastal, arid, and cold areas to control wind and to retard wind driven sediments. As geological and resource exploration and exploitation advances further into increasingly less hospitable environments, such as the prospect of exploration for oil and gas in Arctic region like the northern Norway, there is a strong need to design an optimal porous fence system creating a habitable environment from harsh climate for offshore platforms.

Airflow through a porous fence is a dynamic process that involves interactions between the fence and the air, which the oncoming air velocity does not simply decrease after passing though the fence. Figure 1 illustrates the difference of airflow profiles leeward of porous fences with different porosities [1]. When the porosity is above a critical level, the bleed flow dominates and the airflow in the leeward side of the fence is generally in the same direction as the windward flow shown in Figure 1 (top). When the porosity is below the critical level, the leeward airflow directly behind the fence reverses, resulting in a region of recirculating air shown in Figure 1 (bottom). The researchers [1-4] have found that the presence of both the bleed flow passing through the porous holes and the displaced flow diverted over the fence formed a complex airflow field behind. A high velocity region was

formed above the fence. Flow separation was initiated from the top of the fence and the separation lines extended downwind. For a typical wind protection porous fence that its porosity is in the range from *0.10* to *0.35*, airflow leeward of porous fences has many similar characteristics such as acceleration, deceleration, separation, reverse and recirculation. A significant feature for airflow leeward of such kind of porous fences is to create a wake region where airflow is accelerated downwind by downward transfer of momentum from the overlying layers with higher air velocities, and eventually airflow will be recovered to freestream flow at a certain distance leeward. In conclusion, porous fences change flow velocity, pressure distribution, and energy (i.e. turbulence level and heat transfer) in the surrounding environment.

The performance of a porous fence is generally evaluated by the reduction of wind velocity over its effective shelter distance [2, 4]. A maximum wind reduction for a typical wind-protection porous fence may result in a shortened shelter distance due to the involvement of high shear rate, large pressure gradient and high turbulence intensity, which implies that optimizing a fence performance, should balance these two contradictory factors.

Overall porosity is the ratio of the area of the opening in the fence to the total area of the fence, which has been widely recognized as the most influential structural parameter influencing the performance of porous fences as shown in Figure 2 [5]. From Figure 2, if the reduction of wind velocity is required to *70%* of oncoming wind velocity, the optimum fence porosity was in the range between *0.22* and *0.33*, where the effective shelter distance extended eight to ten times of the fence height. Therefore, an optimum porosity for porous fences is the key parameter in the optimal fence design [3]. Nevertheless, many other factors including the arrangement of porous holes (i.e. shape, size and distribution), the configuration of fence panel itself, and the surrounding environment, etc. need to be considered in the optimization. All of which will have non-negligible impacts on the performance of a porous

fence [4, 6,7].

Study on the use of porous fences and their interaction with the environment is still an ongoing subject to scientific and industrial field even today. Physical experiment including full scale and scaled wind tunnel measurements is the first mean employed with the providence of fundamental knowledge for the study of the optimization of fence performance. Physical experiments involve production and instrumentation located in an area that may or may not have to be prepared prior to installation to create the correct conditions, which are usually expensive and laborious. Full-scale experiments have difficulties in finding controlling environments, and may be inaccessible to extremely harsh weather conditions. Scaled wind tunnel experiments are cheaper and more accessible than full-scale experiments as the environment can be controlled. However, the scaled model experimented in the wind tunnel should have geometric, kinematic and dynamic similarity with the real application. Attempts have been made by many researchers. Snyder [8] proposed a concept of the critical non-dimensional boundary condition that should be identical between the scaled model and the real engineering structure to maintain the similarity, which the testing wind tunnel should have a large span of the test section with adjustable floor to simulate various atmospheric boundary layers in need. Townsend [9] found that the scaled flows were dynamically similar to the full-scale prototype if the Reynolds number was equal or greater than the minimum independent value named as Reynolds Number Independence. White [10] suggested that Reynolds Number Independence would be achieved when the roughness Reynolds number is greater than *2*. The similarity requirements are difficult to satisfy simultaneously that remain a problematic issue even today. As such, it may be questionable if the scaled model is able to yield similar result to the full-scale prototype.

The difficulty of accessibility under extremely harsh weather conditions and the

disadvantage of high cost in testing equipment and labor and the limitation of testing facilities for these physical experiments, motivate computational fluid dynamics (CFD) technique as an effective, cheap and alternative mean in the fence study nowadays [11, 12]. The applicability of CFD techniques has been succeeded in fluid and thermodynamics engineering fields [13-18], which backs its application for the study of porous fences [6, 19-21]. In the early days, two-dimensional (2D) modelling was often used. For example, Wilson [21] used the Reynolds-Averaged-Navier-Stokes (RANS) equations to introduce a momentum sink involving the fence resistance coefficient to simulate a porous barrier. Benefiting from the rapid development of computing power and the availability of cheap hardware and commercial CFD software, three-dimensional (3D) modelling becomes a preferable choice at the present. For example, Giannoulis et al. [19] employed a 3D model to investigate airflow around a raised permeable panel, and the numerical results showed good qualitative and quantitative agreement with the comparing full-scale experimental data. The evident reason is that 3D modelling can provide comprehensive information of flow structures around porous fences within a calculation domain if the numerical model is sound. Nevertheless, 2D modelling is still popular due to the advantages of simple and fast simulation at low computational cost, although it provides information limited in Iso-planes only.

The presence of a porous fence results in an impingement region. Excessive turbulence is generated and downstream wake and separation zones are created in such a region [2, 4]. All of which are problematic for the numerical modellings solved by RANS equations. Wilson [21], using the data of Bradley and Mulhearn [22] as a benchmark for comparison, applied constant viscosity, mixing length, $k-\varepsilon$ and Reynolds stress models to numerically simulate a full size porous fence/shelter in 2D. Of interest was that all of the models examined predicted similar results but could not re-produce an accurate flow profile

downstream of the fence. A more modern approach involve using Large Eddy Simulation (LES), which numerically accounts for the larger scales of turbulence that are more likely to be inhomogeneous. A few LES examples exist in the examination of porous fences with limited improvement of accuracy and high computational cost [23, 24]. Hence, the numerical approximation and parameterization of the flow equations and the ambiguity in describing boundary conditions will introduce error on accuracy and may lead to numerical predictions in question. These require CFD models to be validated against the related physical experiments [14, 15].

In this paper, the porosity of the testing fence is deliberately chosen as *0.27* that is in the range of optimum porosity to represent a typical wind-protection fence. Since the investigating case was subjected to single-phase airflow through a 'thin' fence ($thickness/height = 0.02$ ) at different low velocities. The impact of heat transfer was negligible and therefore not considered here. The evaluation of 2D and 3D modelling airflow around a porous fence is presented with corresponding wind tunnel experiments. The presented CFD models are easy to be constructed and yield quick solutions at low computational cost. The CFD models demonstrate the feasibility as an effective supplementary tool applying to the optimization of porous fence design and application, and are potentially applicable to different scenarios such as different types of fences and different environments, including the potential to expand the models to address heat transfer problems.

***CORRESPONDING WIND TUNNEL EXPERIMENT***

The physical experiment was conducted in an environmental wind tunnel with the span of test section of *1m* wide, *1m* high and*14m* long. Figure 3 depicts the experimental set-up. The testing porous fence (width *0.75m*, height *0.15m* and thickness *0.003m*) is oval-holed uniformly distributed in a planar plane, and its porosity is *0.27*. The testing fence was

installed at *6.75m* away from the leading edge of the test section, and perpendicular to the main flow direction, where a fully turbulent boundary layer should be developed at the fence position [2, 19, 25]. A DA-650 ultrasonic anemometer (UA) was attached to a 3D movable traverse controlled electronically. The experimental data yielded by the UA were automatically recorded onto a computer.

The UA allowed three dimensional velocity components (*u*, *v* and *w*) to be measured in a time duration of *10* seconds with a resolution of *0.01* seconds, which meant each velocity component was obtained by taking the average of *1000* continuous values. $u$, $v$ and $w$ represent velocity component in longitudinal, vertical and lateral direction, respectively. The fluctuation of *u* is expressed as $u'$, and can be obtained as the following:

$$u' = \frac{1}{N-1}\sum_{i=1}^{N}(\bar{u} - u_i) \tag{1}$$

where, $u_i$is the instantaneous $u$ at $i$ measuring times, $N$ is the total measuring times, and $\bar{u}$ is the mean $u$ calculated as:

$$\bar{u} = \frac{\sum u_i}{N} \tag{2}$$

The rest two fluctuations of $v'$ and $w'$ can be calculated in the similar way.

Therefore, the turbulent kinetic energy per unit mass *k* can be acquired as:

$$k = \frac{1}{2}\left(\overline{u'^2} + \overline{v'^2} + \overline{w'^2}\right) \tag{3}$$

In the convenience of comparing numerical results with experimental results, a fully turbulent flow developed at the fence position must be ensured. As such, the wind velocity profile will obey a logarithmic or a power-law profile. Such an investigation was carried out before the fence in position. Three cases corresponding to inlet velocities of 8m/s, 10m/s and 15m/s were investigated, named as C1, C2 and C3, respectively. The inlet velocities were maintained through the control system of the wind tunnel. As kinematic viscosity of air is affected by temperature, the experimental data were taken only after the temperature inside

the wind tunnel was to be stable. The inside temperature was monitored in each case.

To ensure a fully turbulent flow developed at the fence position, The Reynolds number $Re$ has been examined firstly by:

$$Re = UL/v_k \tag{4}$$

where, at temperature 5°C, the kinematic viscosity of air $v_k$ was 1.40E-05m$^2$/s, the maximum velocity $U$ to the fence position was 8m/s, 10m/s and 15m/s, and the distance from the lead edge of the test section to the fence position is the characteristic length $L$=6.75m. Table 1 listed the calculated $Re$ at the fence position for these three cases that indicated that a fully turbulent flow has been developed at this position for all of the cases [26].

Since the airflow was turbulent for all cases, based on $Re$ the thickness of boundary layer $\delta_T$ at the fence position can be estimated using Eq. (5) [27] and are also given in Table1:

$$\delta_T = 0.382L/Re^{0.2} \tag{5}$$

The wind velocity profiles in the vertical direction at the fence position were measured by a Pitot static tube, which was attached to a traverse at the central line of the wind tunnel at a distance of 6.75m from the leading edge of the test section, and connected to a multi-tube manometer. The velocity data were obtained by moving the traverse at 5mm step height in a range from 5mm to 200 mm (in the direction from the wind tunnel floor up). The thickness of boundary layer $\delta$ was obtained at the edge of the boundary where the velocity reached 99% of the freestream velocity listed in Table 1 also. It can be found that the measured $\delta$ and the estimated $\delta_T$ are fairly close, which also indicates a fully turbulent flow developed at this position. Figure 4 shows the measured wind velocity profiles at the fence position within the thickness of boundary layer. It can be observed that the trend lines (Power

C1, Power C2 and Power C3) were well fitted in power regression type, since all of the R-squared value $R^2$ were close to the value of *1*. From Figure 4, the exponents $\alpha$ were obtained and were presented in Table 1.

To covert the power-law velocity profiles into the logarithmic types, x is expressed as a ratio of measuring height h and the thickness of boundary layer $\delta$, the velocity profiles can be written as follows:

- C1: $u_h = 10.062x^{0.1139} = 7.940(h/0.125)^{0.1139}$ (6)
- C2: $u_h = 12.828x^{0.1199} = 9.877(h/0.113)^{0.1199}$ (7)
- C3: $u_h = 19.387x^{0.1175} = 14.876(h/0.105)^{0.1175}$ (8)

Table 1 summarized the data with regard of the examinations of wind velocity profiles, which demonstrated that the wind tunnel has produced wall-bounded fully developed turbulent flow at the fence position.

## *COSIDERATIONS OF CFD MODELLING*

### *Geometric CFD Model to Corresponding Wind Tunnel Experiment*

The geometric models for CFD were created in ANSYS FLUENT workbench. The domain size is identical to the full span of the test section of the wind tunnel. The size of the numerical domain for 2D model was *14m* long and *1m* high. For 3D model, it was *14m* long, *1m* wide and *1m* high.

In the 3D model, the configuration of the numerical fence model was identical to the testing fence, where the arrangement of porosity i.e. size, shape and distribution of holes was the same as the physical fence. The fence was placed at the distance of *6.75m* from the leading edge of the test section (x-y plane), and was centered in the y-z plane to replicate the location used in the experimental tests. Figure 5 shows the geometric 3D model. Since the numerical domain was symmetrical to the y-z plane at *x=0m*, the domain as reduced to half to

save computing expense.

In the 2D modelling, the characteristics of the porous fence were not physically modelled. It is usually treated as a pressure discontinuity surface by applying a porous medium condition (porous jump or porous zone), where an additional momentum source term is added to the standard fluid flow equations as the following:

$$S_i = -\left(\sum_{j=1}^{3} D_{ij}\,\mu v_j + \sum_{j=1}^{3} C_{ij}\,\frac{1}{2}\rho|v|v_j\right) \quad (9)$$

where, $S_i$ is the source term for the $i^{th}$ (x, y or z axial direction) momentum equation, $|v|$is the magnitude of the velocity, $\mu$ is the laminar fluid viscosity, $\rho$ is the density of the fluid, and $D$ and $C$ are prescribed matrices. It is composed of two parts: the first term on the right-hand side in Eq. (9) is a viscous loss term, and the second term on the right-hand side is an inertial loss term. $S_i$ is absorbed from fluid flow as a momentum sink, which attributes to the pressure gradient in the porous cell, and creates a pressure drop that is proportional to the fluid velocity in the cell.

The testing fence in the present study is thin with uniformly distributed porous holes, which can be considered as a simple homogeneous and thin 'membrane'. ANSYS FLUENT has a specific treatment for such a 'membrane' named as a porous jump. Eq. (9) can be further simplified to describe the pressure change in the form of a combination of Darcy's Law with an additional inertial loss term:

$$\Delta p = -\left(\frac{\mu}{a}V + \frac{1}{2}C_2\rho V^2\right)\Delta m \quad (10)$$

where, $a$ is the permeability of the fence, $C_2$ is the pressure-jump coefficient, $V$ is the velocity normal to the porous fence, and $\Delta m$ is the thickness of the fence.

The porous jump is applied to a face zone instead of a cell zone. This one-dimensional simplification was highly recommended as it is more robust and yields better convergence

[28].

Since the porous fence was subjected to single-phase airflow, there were only three input parameters to be configured as follows:

*The thickness of the fence* $\Delta m$.

*The face permeability* $a$ *:* for turbulent flow around a perforated plate like planar porous fences, the viscous loss term can be neglected [15, 28]. Hence, $a$ for the fence was assigned a great value as *1E+20*$m^2$ to eliminate the viscous loss term $\frac{\mu}{a}V$ in Eq. (10).

*The pressure-jump coefficient* $C_2$: it was associated with the resistance coefficient or pressure loss coefficient $k_r$ calculated as follows:

$$C_2 = k_r/\Delta m \tag{11}$$

$$k_r = 0.52(1-\beta^2)/\beta^2 \tag{12}$$

where, $\beta$ is the porosity of the fence.

Porous cells for a porous jump are treated as *100%* open to the domain, which differs the fact where the fence is only partially open to the flow. Presuming the flow rate unchanged with or without the fence, $u_{27\%open} = 3.7u_{100\%open}$.Hence, $k_r$ needed to be adjusted as $k_R$:

$$k_R = k_r\left(u^2_{27\%open}/u^2_{100\%open}\right) \tag{13}$$

Table 2 lists the calculated variables for the porous jump (the fence).

***Model Sensitivity Analysis***

Model sensitivity analysis is important in numerical simulations. The values of model parameters, the computations, and the input values of variables are prone to many sources of numerical uncertainty. Therefore, the sensitivity of a model outputs to the perturbation in CFD simulations must be analyzed. Model sensitivity analysis may be performed on mathematical and computational models to determine the sensitivity of model outputs to the

uncertainty of input variables, computations, and parameter values [29]. By performing sensitivity analysis on an application, the insight of model stability is understood. If the results from the analysis are not stable, it needs to revise the designed computations.

In the present CFD simulations, the mathematical model was governed by the RANS equations, describing time-averaged motion of fluid flow. The additional unknown variables (called Reynolds stresses) exhibited from the RANS were solved by the Standard $k-\varepsilon$ turbulence model. It is the most widely used and validated turbulence model with applications ranging from industrial to environmental flows. However, it assumes the turbulent viscosity is isotropic to give a general description of turbulence by means of two partial differential transport equations. Hence, it might be insufficient to predict turbulence for the airflow leeward of the porous fence, where the airflow exhibited strong separations, swirling and rotating with large pressure gradients in the presence. It is well acknowledged that modelling turbulence flow is sensitive to the choice of turbulence models. The fact faces today as the statement: 'it is an unfortunate fact that no single turbulence model is universally accepted as being superior for all classes of problems. The choice of turbulence model will depend on considerations such as the physics encompassed in the flow, the established practice for a specific class of problem, the level of accuracy required, the available computational resources, and the amount of time available for the simulation.'

The model sensitivity analysis in this paper focused on the discussions of mesh independence. Mesh independence is that the numerical solution must be ensured to be independent of the mesh resolution. Any CFD simulation must conduct mesh independence before taking further actions, because discretization of partial differential equations into ordinary difference equation is influenced by the spatial cell size. An ideal mesh should be where a solution is just independent of the spatial cell size. A good quality of mesh should be efficient and economic which is as close to the ideal mesh as possible.

Quadrilateral elements were applied in the entire domain in the 2D model shown in Figure 6. The denser elements were arranged in the region close to the floor by applied the height of the first layer of 1mm with the bias factor of *1.2*.

In the 3D modelling shown in Figure 7, the denser elements were created in the regions near the fence and the floor. The region close to the wind tunnel floor was constructed by tetrahedron prism elements. The rest regions by tetrahedron elements.

During the mesh sensitivity analysis, the velocity magnitudes and turbulence intensities at the positions of comparing vertical lines (y-axial) were selected as the monitoring variables. These positions of comparing lines were carefully chosen to reflect the characteristics of flow leeward of the fence. The vertical line at $x = 0.2m$ was in the close fence region where vortex may involve, the lines at $x = 1.0m$ and $1.8m$ were in the fence effective zone likely having reverse cells and wake flows, and the line at $x = 3.5m$ was in the internal boundary layer affected region. The initial mesh guess was used by ANSYS FLUENT default mesh, and then increasing the quality of mesh by a factor of 1.5 as the second guess, and so on. When the solution was close to the one solved by the last mesh, decreasing the quality of mesh by a factor of 0.5 until the mesh independence was identified. For the 2D model, the mesh with *0.28* million elements has reached the grid independence. For the 3D model, the mesh with *1.5* million elements has achieved the solution independent.

ANSYS FLUENT [28] recommends with regard of mesh quality that the minimum orthogonal quality should be greater than *0.1*, and the maximum skewness value should be less than *0.95*. The greater value of the orthogonal quality close to *1.0*, the better quality of the mesh. However, for the skewness value, vice versa. The minimum, average and maximum skewness value for the 2D model was 2.8E-05, 0.01 and 0.03; and for the 3D

model, 5.0E-04, 0.22 and 0.85, respectively. The minimum, average and maximum orthogonal quality for the 2D model is 1.0, 1.0 and 1.0; and for the 3D model, 0.48, 0.87 and 1.0. All of which were in the favor of the requirements of ANSYS FLUENT.

***Other Considerations***

The conditions of velocity inlet were used from the ones of the experiment. At the pressure outlet, the flow field variables were extrapolated from the adjacent interior cells and the normal gradient was vanished. The Gauge pressure was set to zero since the porous fence had no or very minor effect on the airflow at this position, where the airflow was recovered to freestream flow. According to the characteristics of the wind tunnel, turbulence intensity in the freestream was *5%*. Both of the backflow turbulence intensity and the backflow turbulent viscosity ratio were set as *5%* in the simulations. A no-slip condition was applied for all of the walls in the domain. The solution methods adapted SIMPLE (Semi-Implicit Method for Pressure Linked Equations) scheme pressure-velocity coupling, as it is a widely used numerical procedure to solve the Navier-Stokes equations [19, 30].

The convergence criteria were assessed by monitoring the scaled residuals. Additionally, the history of drag coefficient in the longitudinal direction was monitored too.

The solution initialization run the hybrid method with *10* of iterations. The ultimate solution was obtained on the Second Order Upwind discretization.

***RESULTS AND DISCUSSIONS***

***Assessment of CFD Models***

The examining numerical data were taken along the lines corresponding to the ones in the wind tunnel experiment with the purpose of model assessment, where the structures of velocity magnitude and turbulent kinetic energy were compared. The positions of comparing lines were the same as the ones for the mesh sensitivity analysis, where the significant

features of flow regime leeward of the fence will be captured.

In the convenience of comparisons, the presented figures were expressed as follows:

*Axis X*: for velocity investigations, it was expressed as the ratio of the local velocity magnitude $U$ and the free stream velocity $U_0$. For turbulence investigations, the local turbulent kinetic energy was used;

*Axis Y:* it was expressed as the measuring height $h$ normalized by the corresponding fence height $H$.

The simulated results revealed that the structures of velocity and turbulence appeared quite similar feature among the cases of C1, C2 and C3. As such, the case of C1 was discussed in this paper. Figure 8 presents the comparisons of velocity magnitudes in the flow regime leeward of the fence at the inlet velocity of 8m/s. Both of 2D and 3D simulations predicted the structure of velocity magnitude in a good agreement with the experimental results in general, which implies that the CFD models performed well in velocity predictions.

There was a difference between the experimental and numerical results in the region of $h/H > 2.0$, the values of experimental data appeared smaller. This was because the top wall of the wind tunnel actually affected the flow that restrained the flow acceleration. In the simulations, the top wall was treated as a no-slip wall with coarse mesh in place. Since the structure of flow within the effective fence zone was of main concern, such difference can be considered as acceptable.

The comparisons of turbulent kinetic energy leeward of the fence at the inlet velocity of 8m/s are displayed in Figure 9. It shows that both 2D and 3D simulations over-predicted turbulent kinetic energies compared with the experimental results. The 2D model predicted the greatest values. However, the numerical predictions appeared a similar pattern to the experimental ones. It increased the value from the floor and reached a maximum value in the

region of $0.7 < h/H < 1.5$, after which its value started to drop, and beyond the region $h/H > 3.0$, the value closed to each other and appeared to be recovered to the freestream flow. The noticeable discrepancies indicate the uncertainty on both the experiments and the numerical modellings.

***Uncertainty Discussion***

*Uncertainties on the experiment*: the applied UA would introduce error of accuracy to velocity measurements and consequently to turbulence. The accuracy of the velocity component for example $u_i$ is expressed as:

$$u_i = u_i(1 \pm \sigma) \tag{14}$$

where, $\sigma$.is the accuracy of the UA.

The mean-squared deviation $\overline{u'^2}$ is:

$$\overline{u'^2} = \frac{1}{N-1}\sum_i^N(\bar{u} - u_i)^2\,(1 \pm \sigma)^2 \approx \overline{u'^2}\left(1 \pm \frac{4N\sigma}{N-1}\right) \tag{15}$$

The above statements are applicable to $v_i$,$w_i$, $\overline{v'^2}$ and $\overline{w'^2}$.

Substitute these parameters into Eq. (3), accuracy of $k$ based on the measurement of velocity components is:

$$k = \left(1 \pm \frac{6N\sigma}{N-1}\right)k \tag{16}$$

$\sigma$ for the applied UA is *1%*. In the experiment, $N$ is times of *1000*. As such, $N/N-1$ is close to *1*. Hence, error of accuracy on turbulent kinetic energy is amplified six times bigger than the one on velocity, which is quite significant.

The UA used in the experiment is an intrusive instrument, which would distort the wind field at the measuring points that induced the errors into velocity data. Although the ultrasonic anemometer enabled to measure three dimensional velocity components in a fine time resolution, the produced data were still time-averaged that might be still insufficient to capture the complex nature of turbulence. Such uncertainties cannot be justified under the

present experimentation.

*Uncertainties on CFD modelling:* the CFD modellings were good in predicting the structure of velocity but not so well in predicting the structure of turbulence. The applied standard $k-\varepsilon$ turbulence model exposed its weakness in simulating turbulence, which was the main cause induced uncertainty on the CFD modellings. The weakness in predicting turbulence for the available two-equation based turbulence models including $k-\epsilon$ and $k-\omega$ models, has been recognized in the porous fence research field. Improvement is needed in the future work.

Second to the turbulence model was the application of no-slip condition, which might introduce errors for the wall modelling. Particularly for the porous fence, neither the porous jump for the 2D model nor the no-slip condition for the 3D model was sufficient to model large gradients involved variables induced by considerable numbers of porous holes. It is better to assign a scalar wall function in such region in the future work.

***Post Process***

The post process of 3D modelling has demonstrated its power and convenience in acquiring data in need. Compared with the wind tunnel experiment and 2D modelling, it can conduct graphic and numerical investigations at any position within the entire domain, and can use the function calculator to obtain new variables, make tables and produce reports.

Figure 10 shows the structures of air velocity vectors simulated by 2D and 3D models. It can be observed that the displaced flow diverted over the fence accelerating the air velocities and forming an overflow region. The bleed flow passing through the porous holes decelerating the air velocities and creating a fence protection zone. The displaced flow and the bleed flow formed a wake region leeward of the fence, which involved flow recirculation

and a small vortex stagnation right behind the fence. The velocity profile became more uniformed in shape with increasing the downwind distance, and eventually recovered to the freestream velocity. Both of them successfully presented the similar features that were in good agreement with the ones founded from physical experiments [2]. The characteristics of flow regime around the fence can also be observed from the velocity streamlines. Figure 11 presents the structure of velocity streamlines within the entire domain in 3D modelling, which is superior to the 2D model that only displayed in Iso-plane.

Figure 12 shows the contours of total pressure in the relevant planes. The top is the contour of total pressure in the symmetry wall with a low-pressure zone created leeward of the fence. The left under is the amplified contour of total pressure in the symmetry wall, where the porous holes are in absence. The right under is in the x-y plane with 7.5mm offset from the symmetry wall, where the porous holes are in presence. It can be observed that the porous holes mitigated the pressure drops in both sides of the fence, while creating large pressure gradients insider the holes and leeward of the fence. The presence of considerable amount of holes in a porous fence will create a complex distribution of shear on the fence surface when encountered airflow. These shears result in producing large gradients to pressure, velocity and turbulence. It has been acknowledged that the distribution of fence shear is an important parameter in determining the feature of a porous fence. However, it has been difficult to be investigated by physical experimental techniques. It cannot be addressed under 2D CFD modelling either. The 3D modelling can provide such complementary information in detail. Figure 13 is the distributions of wall shear in two sides of the fence. It was observed that the front face presented far greater shear than the back face did. The value of shear was increased with the increase of the vertical height in the fence, which indicates that higher wind velocity encountered, higher wall shear created.

Figure 14 is the volume rendering of the turbulent kinetic energy in the domain. It was

obtained with the resolution of *30* and the transparency of *0.2*. The volume rendering technique enables to visualize the CFD data for better understanding the processes in the simulation, and helps to assess the quality and efficiency of mesh. In Figure 14, the top shows that the concerned turbulent kinetic energies were captured in the effective element volumes. The under shows the changes of turbulent kinetic energies inside the holes captured in a good resolution. It also demonstrated that the elements with relatively large volumes have been arranged in the regions where the turbulent kinetic energy has trivial changes. The volume rendering has revealed that the current arrangement of mesh is sufficient and efficient.

***CONCLUSIONS***

Airflow around a porous fence has been simulated in 2D and 3D models. The models were easy to be constructed and yielded quick solutions at low computational cost. Both of the 2D and 3D models were evaluated against corresponding wind tunnel experiments. Both of them have predicted the structure of wind velocity in good agreement with the experimental results. Both of them have over-predicted the level of turbulence leeward of the fence compared with the experimental results. In general, the models are applicable to porous fence research.

3D modelling demonstrates its superiority in providing comprehensive information with great convenience within the entire domain. Some useful information, such as the distributions of shear stress and pressure on the fence surface, etc. is unlikely to be obtained from 2D modelling and physical experiment. Nevertheless, 2D modelling also shows its strength in easier construction of numerical model and lower computational cost. Hence, the selection of CFD model must be dependent on the application and the purpose of analysis. Finally, physical experiment is not dispensable, as CFD technique is a supplementary tool in today's porous fence study.

The demonstrated feasibility implies that the CFD models are potentially applicable to address issues like heat transfer. It however must be aware that the present 2D model is not applicable. If heat transfer is of concern for the 2D model, the porous fence must be treated as a porous zone instead of a porous jump.

***ACKNOWLEDGEMENT***

Norwegian Research Council financed the work under project number 195153 (ColdTech). The authors also acknowledge the support from the Arctic University of Norway.

***NOMENCLATURE***

$a$ permeability of the fence, $m^2$

$C_2$ pressure-jump coefficient, $1/m$

*CFD* computational fluid dynamics

$H$ fence height, $m$

$h$ measuring height, $m$

$k$ turbulent kinetic energy per unit mass, $m^2/s^2$

$k_r$ pressure loss coefficient, dimensionless

$k_R$ adjusted pressure loss coefficient, dimensionless

$L$ reference length, $m$

*LES* large eddy simulation

$\Delta m$ thickness of the fence, $m$

$N$ total measuring times

$\Delta p$ pressure drop, $N/m^2$

$Re$ Reynolds number, dimensionless

$R^2$ R-squared value, dimensionless

*RANS* Reynolds-Averaged-Navier-Stokes

$S_i$ source term, $kg/ms$

$U$ local wind velocity magnitude, $m/s$

$U_0$ free stream wind velocity, $m/s$

$u_h$ wind velocity at measuring height of $h$, $m/s$

*UA* ultrasonic anemometer

$u$ longitudinal velocity component, $m/s$

$V$ velocity normal to the fence, $m/s$

$v$ vertical velocity component, $m/s$

$v_k$ kinematic viscosity of air, $m^2/s$

$w$ lateral velocity component, $m/s$

*x* a ratio of measuring height and the thickness of boundary layer in the equations or the width of the airflow domain

*y* the height of the airflow domain

*z* the length of the airflow domain

***Greek Symbols***

$\alpha$ power exponent, dimensionless

$\beta$ porosity of the fence, dimensionless

$\delta$ thickness of boundary layer, $m$

$\delta_T$ estimated thickness of boundary layer, m

$\mu$ laminar fluid viscosity, $Ns/m^2$

$\rho$ density of fluid, $kg/m^3$

$\sigma$ error of accuracy, %

$\omega$ specific turbulence dissipation rate, $1/s$

$\varepsilon$ turbulence dissipation rate, $m^2/s^3$

***Subscripts***

$_i$ instantaneous data

***Superscripts***

$'$ fluctuation data

$\bar{}$ averaged data



***REFERENCES***

[1] Xu, Y., and Mustafa, M., "Investigation of the Structure of Airflow behind a Porous Fence Aided by CFD Based Vi," *Sensors & Transducers,* vol. 185, no. 2, pp. 149-155, 2015.

[2] Dong , Z. Luo, W. Qian, G. Wang, H., "A wind tunnel simulation of the mean velocity fields behind upright porous fences," *Agricultural and Forest Meterorology,* vol. 146, no. 1-2, pp. 82-93, 2007.

[3] Dong, Z. Luo, W. Qian, G. Wang , H., "Evaluating the optimal porosity of fences for reducing wind erosion," *Science in Cold and Arid Region,* vol. 3, no. 1, pp. 1-12, 2011.

[4] Cornelis, W., Gabriels, D., "Optimal windbreak design for wind-erosion control," *Arid Environments,* vol. 61, no. 2, pp. 315-332, 2005.

[5] Government of Saskatchewan, "Portable windbreak fences," [Online]. Available: https://www.saskatchewan.ca/business/agriculture-natural-resources-and-industry/agribusiness-farmers-and-ranchers/livestock/cattle-poultry-and-other-livestock/cattle/portable-windbreak-fences.

[6] Wang , H., Takle, E. S., Shen, J., "Shelterbelts and windbreaks: mathematical modeling and computer simulations of turbulent flows," *Annual Review of Fluid Mechanics,* vol. 33, no. 1, pp. 549-586, 2001.

[7] Xu, Y., Virk, M., Knight, J., Mustafa, M., "Factors influencing the performance of

porous wind shields," *Applied Mechanics and Materials,* Vols. 321-324, no. 1, pp. 799-803, 2013.

[8] W. Synder, "Similarity criteria for the application of fluid models to the study of air polluion meteorology.," *Boundary Layer Meteorology,* vol. 3, no. 1, pp. 113-134, 1972.

[9] A. Townsend, The structure of turbulent shear flow, Cambridge: Cambridge University Press, 1956, p. 315.

[10] B. White, "Laboratory simulation of aeolian sand transport and physical modeling of flow around dune," *Annals of Arid Zone,* vol. 35, no. 3, pp. 187-213, 1996.

[11] Barlow, J. B., Rae, Jr, W. H., Pope, A., Low-speed wind tunnel testing (third edition), New York: John Wiley & Sons, Inc, 1999.

[12] Kline, S.J., Similitude and approximation theory, New York: Springer-Verlag, 1986.

[13] Beyers , M., Waechter, B., "Modeling transient snowdrift development around complex three-dimentsional structures," *Wind Engineering and Industrial Aerodynamics,* vol. 96, no. 10-11, pp. 1603-1615, 2008.

[14] Blocken, B., "50 years of computational wind engineering: past, present and future," *Wind Engineering and Industrial Aerodynamics,* vol. 129, no. 1, pp. 69-102, 2014.

[15] Bourdin, P., Wilson, J., "Windbreak aerodynamcis: is computational fluid dynamics reliable?," *Boundary-Layer Meteorology,* vol. 126, no. 2, pp. 181-208, 2008.

[16] Kumar, R., Dewan, A., "Computational models for turbulent thermal plumes: recent advances and challenges," *Heat Transfer Engineering,* vol. 35, no. 4, pp. 367-383, 2014.

[17] Sun, D., Xu, J., Chen, Q., "Modeling of the evaporation and condensation phase-change problems with FLUENT," *Heat Transfer Engineering,* vol. 66, no. 4, pp. 326-342, 2014.

[18] Mohammadi, K., Malayeri, M.R., "Model-based performance of turbulence induced structures in exhaust gas recirculation (EGR) coolers," *Heat Transfer Engineering,* vol. 36, no. 7-8, pp. 706-714, 2015.

[19] Giannoulis, A., Mistriotis, A., Briassoulis, D., "Experimental and numerical investigation of the airflow around a raised permeable panel," *Wind Engineering and Industrial Aerodynamics,* vol. 98, no. 12, pp. 808-817, 2010.

[20] Andres, G., Wolfgang , F., Wolfgang, S., Mathias, D., "CFD modelling and validation of measured wind field data in a portable wind tunnel," *Aeolian Research,* vol. 3, no. 3, pp. 315-325, 2011.

[21] J. Wilson, "Numerical studies of flow through a windbreak," *Wind Enineering and industrial Aerodynamcs,* vol. 21, no. 2, pp. 119-154, 1985.

[22] Bradley , F., Mulhearn, P., "Development of velocity and shear stress distributions in the wake of a porous shelter fence," *Wind Engineering and Industrial Aerodynamics,* vol. 15, no. 1-3, pp. 145-156, 1983.
[23] Fang, F., Wang, D., "On the flow around a vertical porous fence," *Wind Engineering and Industrial Aerodynamics,* vol. 67, no. 1, pp. 415-424, 1997.
[24] Patton, E.G., Shaw, R.H., "Large-eddy simulation of windbreak flow," *Boundary-Layer Meteorology,* vol. 87, no. 2, pp. 275-306, 1998.
[25] Raine, J., Stevenson, D., "Wind protection by model fences in simulated atmospheric boundary layer," *Wind Engineering and Industrial Aerodynamics,* vol. 2, no. 2, pp. 159-180, 1977.
[26] Trinh, K.T., "Additive layers: an alternate classification of flow regimes," in *Chemeca 2012: Quality of life through chemical engineering*, Wellington, New Zealand, 2012.
[27] Barlow, J.B., Rae, W.H., Pope, A., Low-speed wind tunnel testing (third edition), New York: John Wiley & Sons, Inc., 1999.
[28] ANSYS, ANSYS FLUENT user's guide, Canonsburg, USA: ANSYS, Inc., 2011.
[29] Campolongo, F., Braddock, R., "The use of graph theory in sensitivity analysis of model output: a second offer screening method," *Reliability Engineering and System Safety,* vol. 64, no. 1, pp. 1-12, 1999.
[30] Gupta, S. K., Ray, S., Chatterjee, D., "Influence of aiding buoyancy on the suppression of flow separation for power-law fluids around a circular object," *Heat Transfer Engineering*, vol. 37, no. 15, pp. 1267-1279, 2016.

**Table1: Variables for the velocity profiles at the fence position**

| Item | C1 | C2 | C3 |
|---|---|---|---|
| Inlet velocity (m/s) | 8 | 10 | 15 |
| $Re$ ($\times 10^6$) | 3.86 | 4.82 | 7.23 |
| $\delta_T$ (m) | 0.13 | 0.12 | 0.11 |
| $\delta$ (m) | 0.125 | 0.113 | 0.105 |
| $\alpha$ | 0.1139 | 0.1199 | 0.1175 |
| $R^2$ | 0.9968 | 0.9993 | 0.9989 |

**Table 2: Variables for the porous jump**

| Item | Unit | Value |
|---|---|---|
| Fence height $H$ | $m$ | 0.15 |
| Porosity $\beta$ | | 0.27 |
| Fence thickness $\Delta m$ | $m$ | 0.003 |
| Pressure loss coefficient $k_r$ | | 6.61 |
| Adjusted pressure loss coefficient $k_R$ | | 90.67 |
| pressure-jump coefficient $C_2$ | $m^{-1}$ | 30224 |
| Face permeability $a$ | $m^2$ | 1e+20 |

*LIST OF FIGURE CAPTIONS*

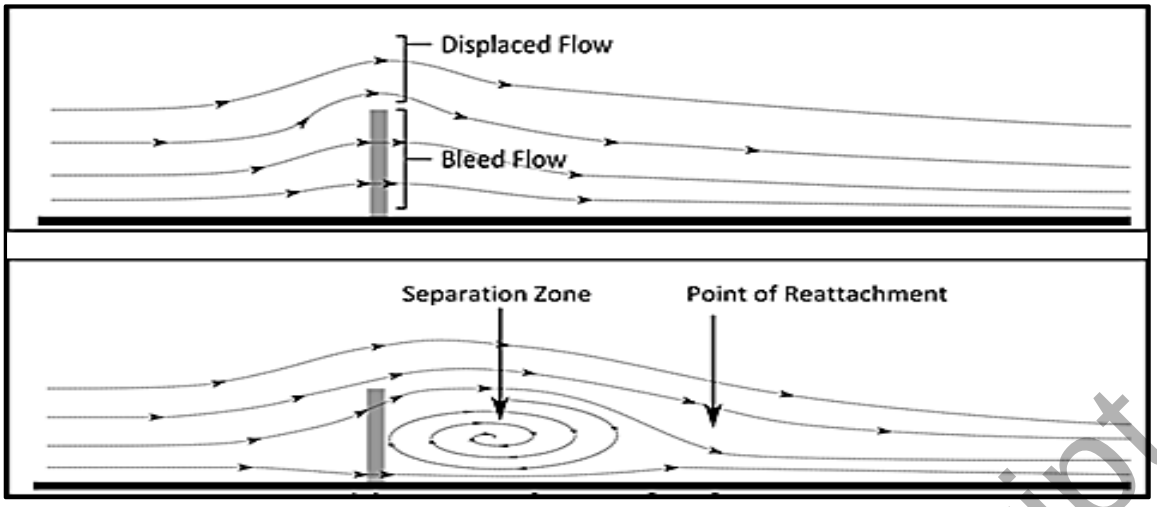


**Figure 1: A typical streamline patterns behind a porous fence when its porosity is below and above a critical level**

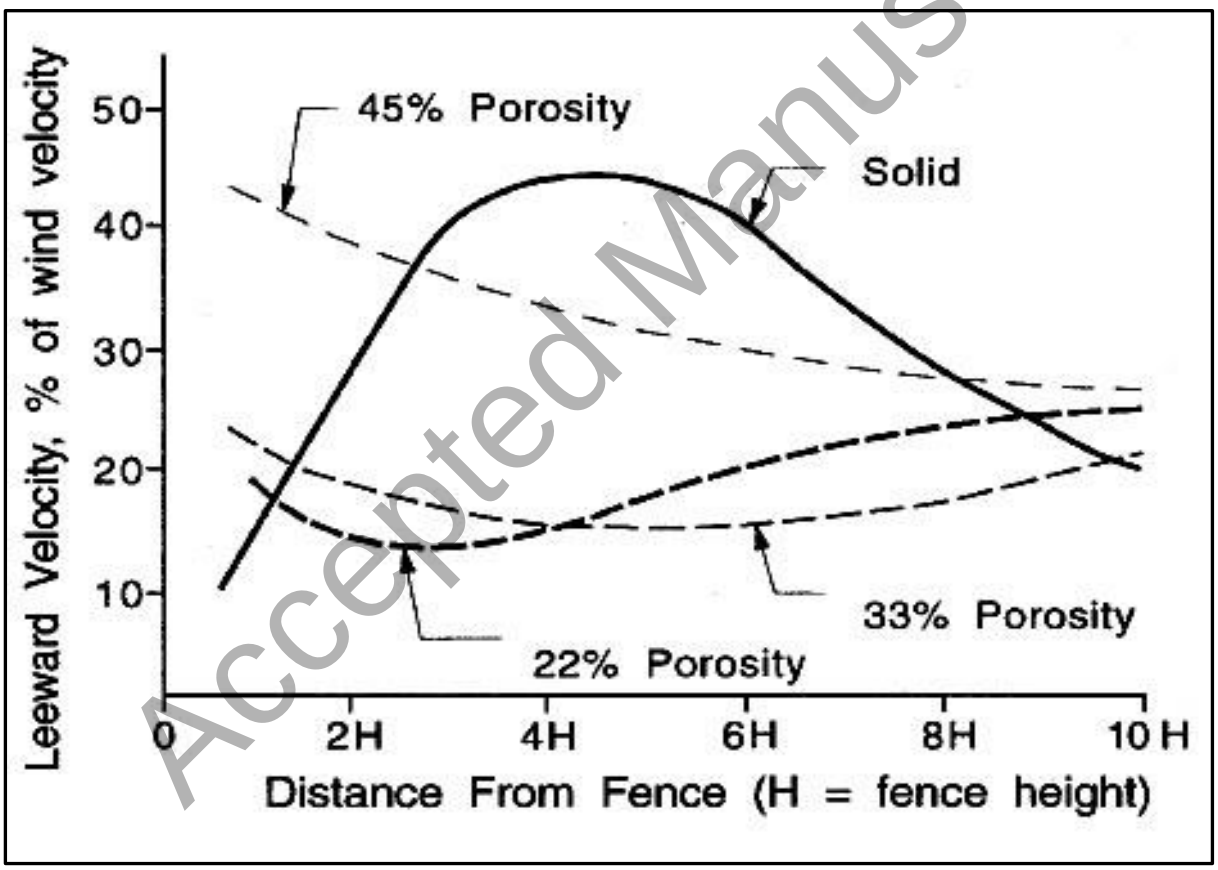


**Figure 2: Reduction of leeward of wind velocity over distance from the fence at different porosities**

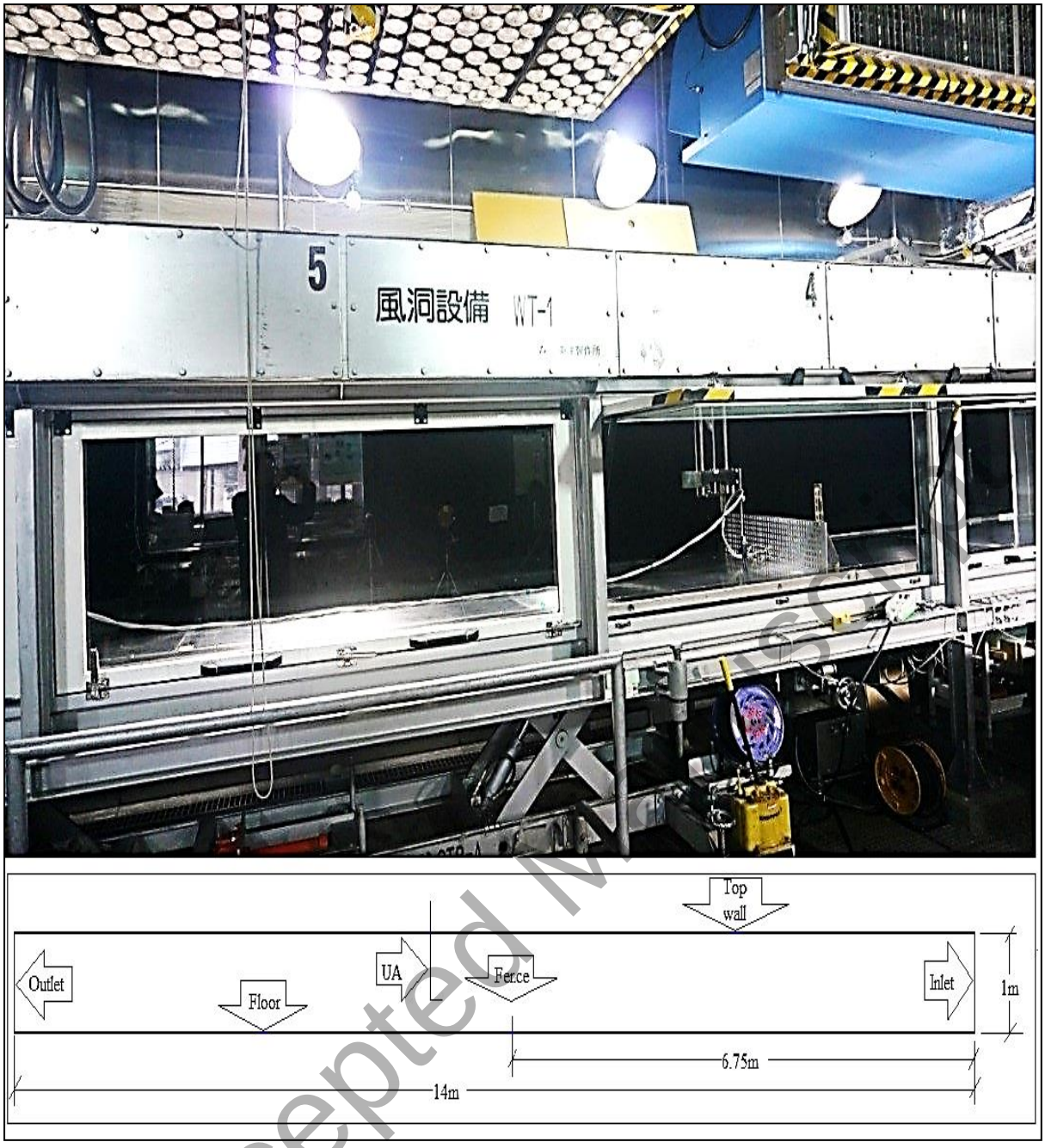


**Figure 3: Wind tunnel experimental set-up**

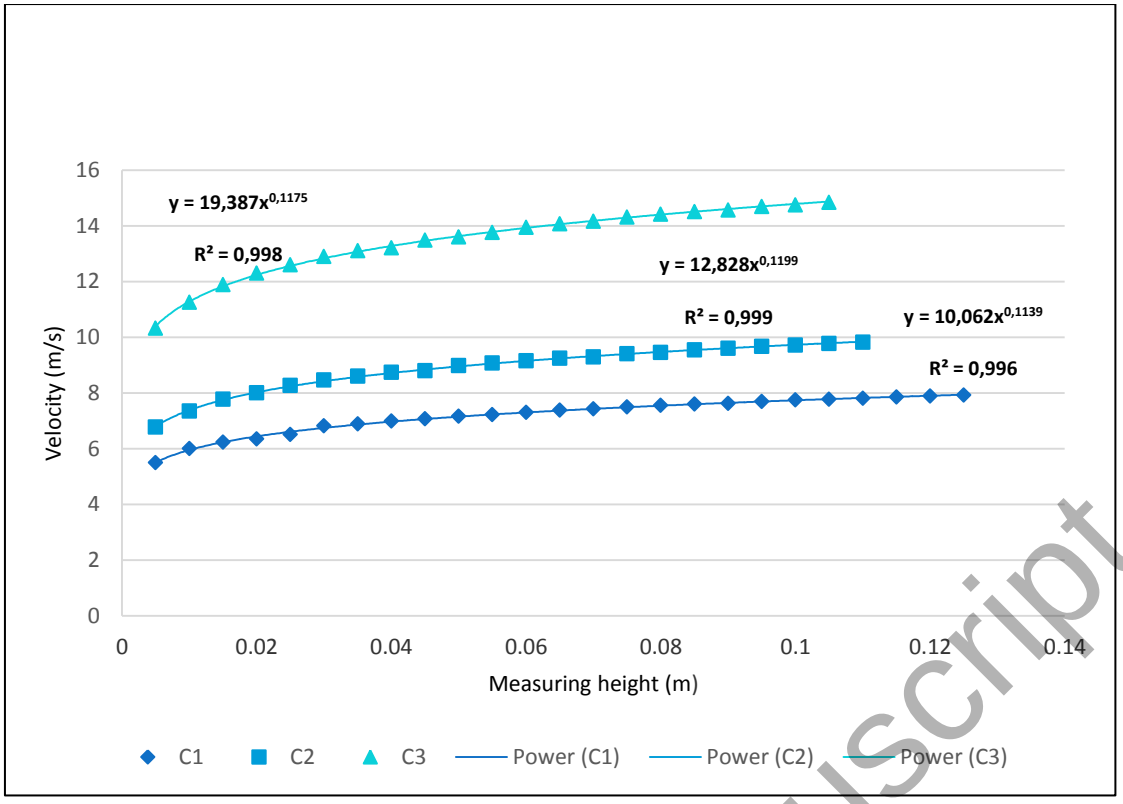


**Figure 4: The wind velocity profiles at the fence position within the thickness of boundary layer**

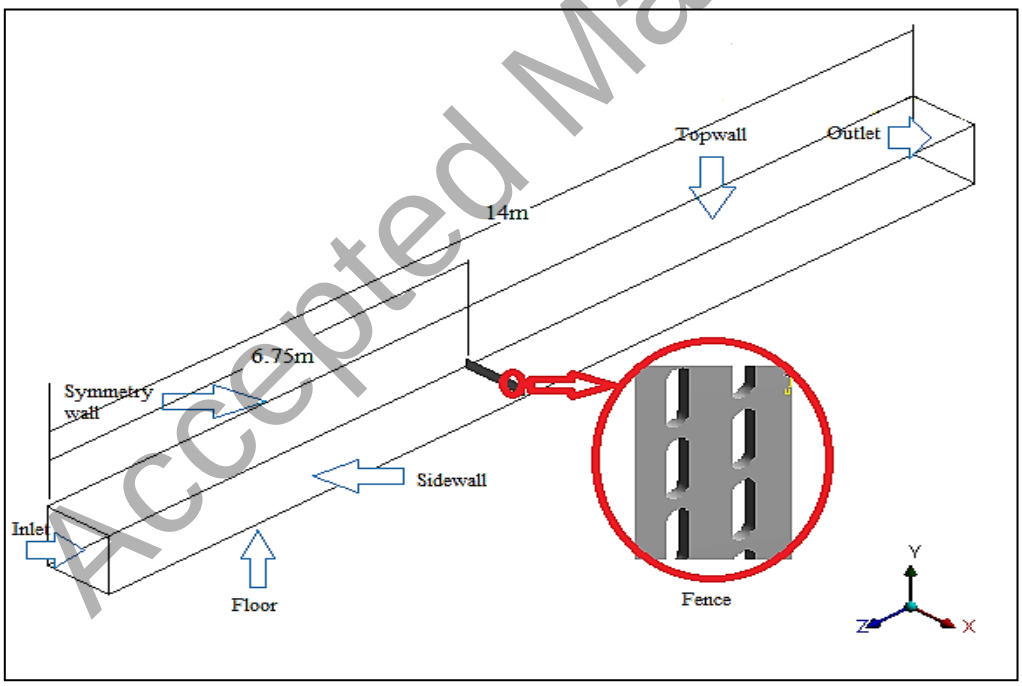


**Figure 5: 3D geometric model**

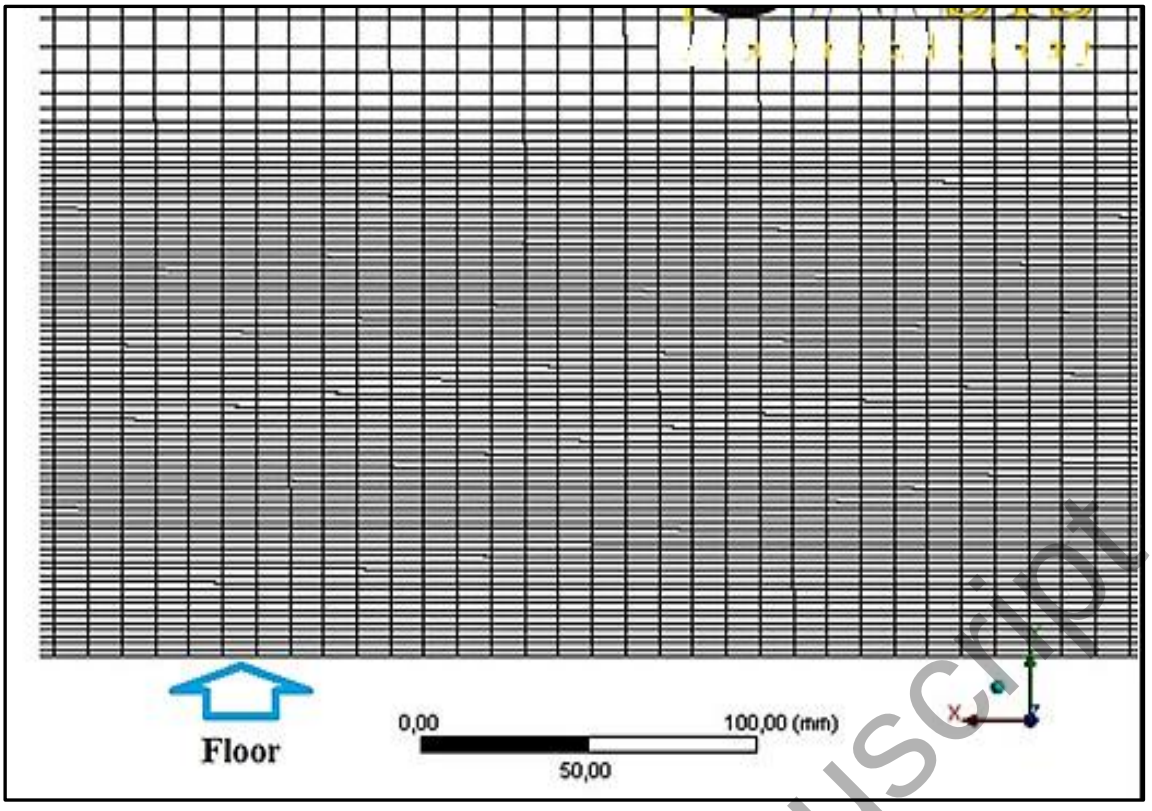


**Figure 6: Meshing close to the floor region for the 2D model**

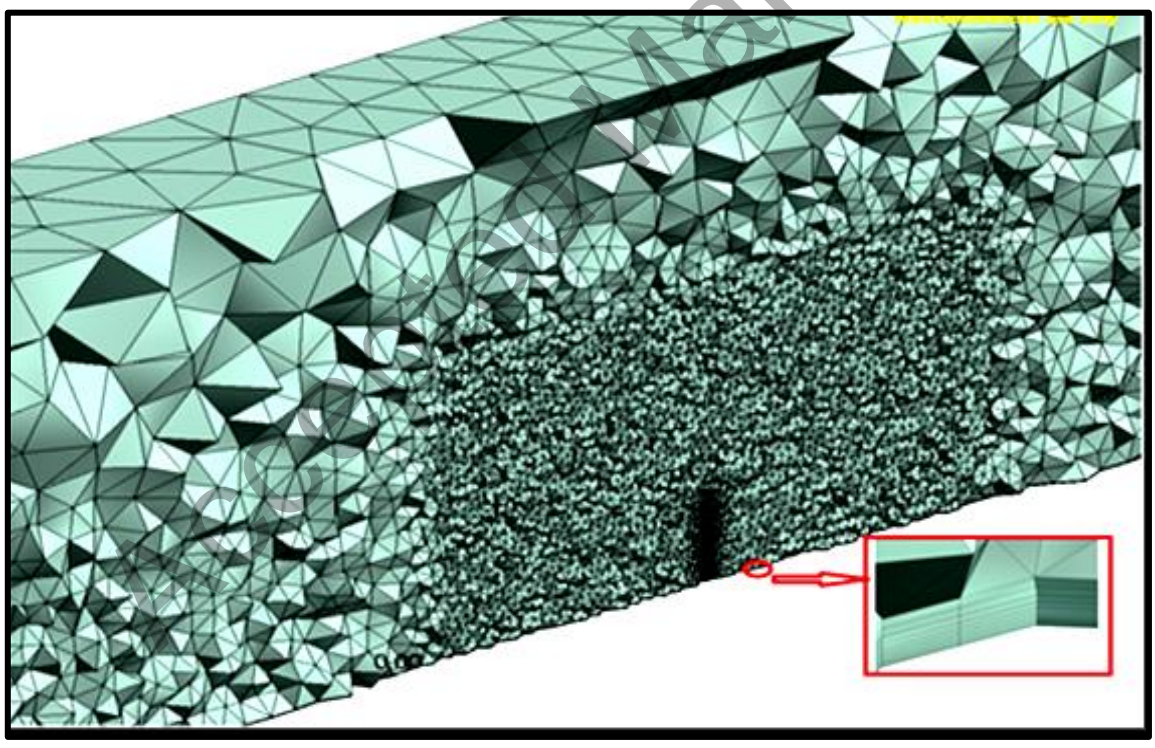

**Figure 7: Meshing in the near fence and floor region for the 3D model**

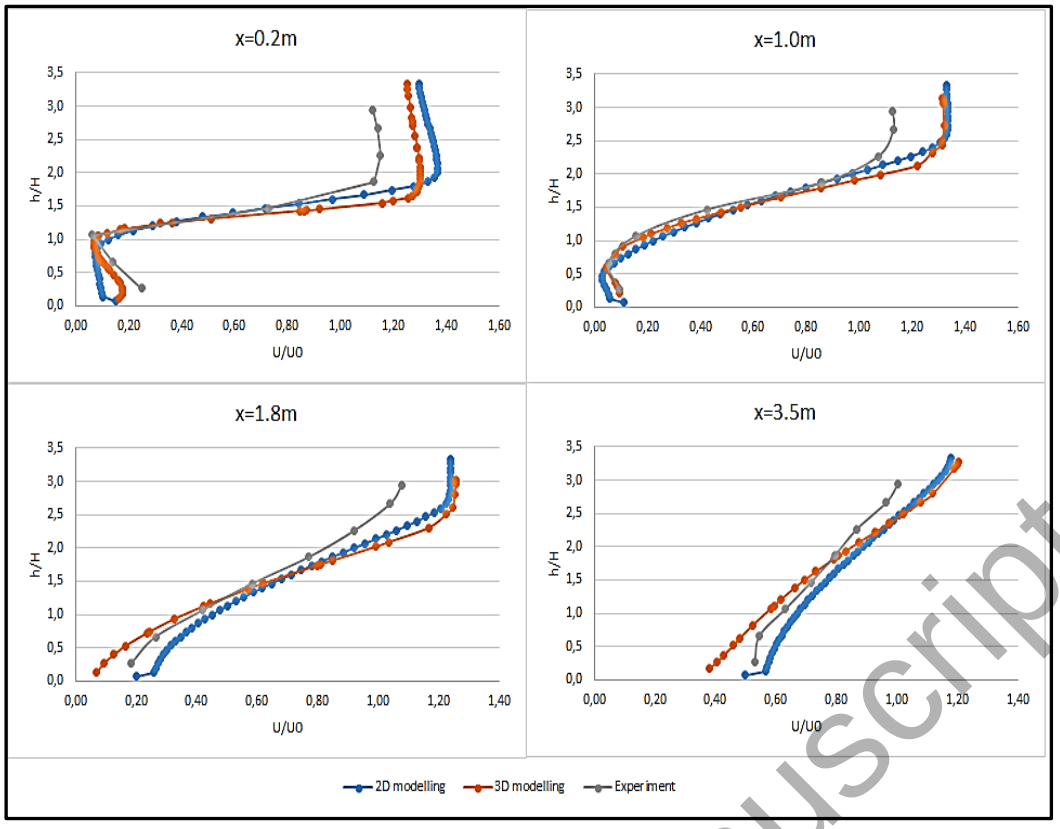


**Figure 8: Comparisons of velocity magnitude in the domain**

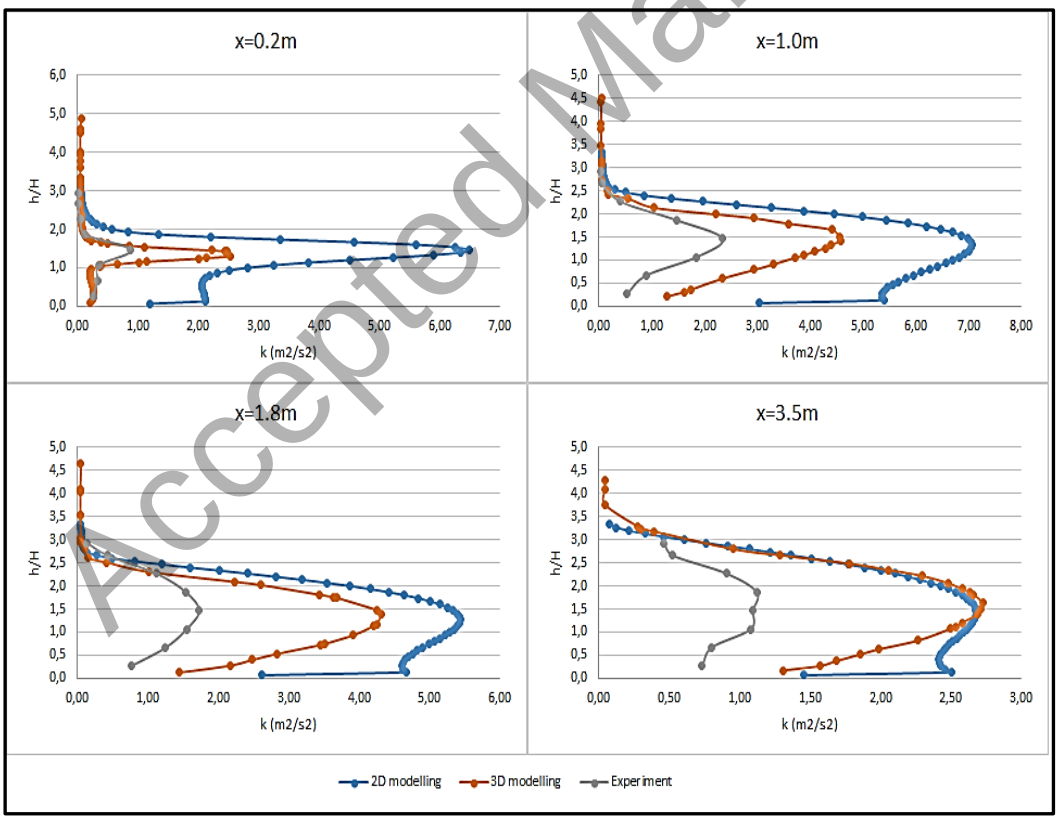


**Figure 9: Comparisons of turbulent kinetic energy in the domain**

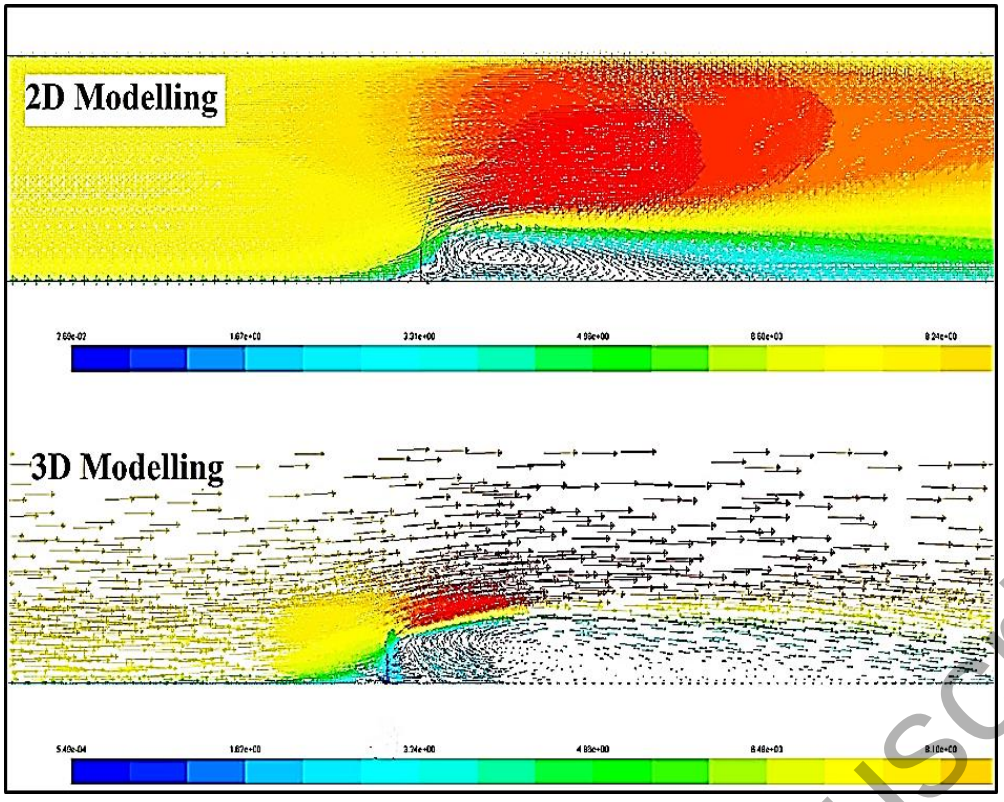


**Figure 10: The structures of velocity vector simulated by 2D and 3D modellings**

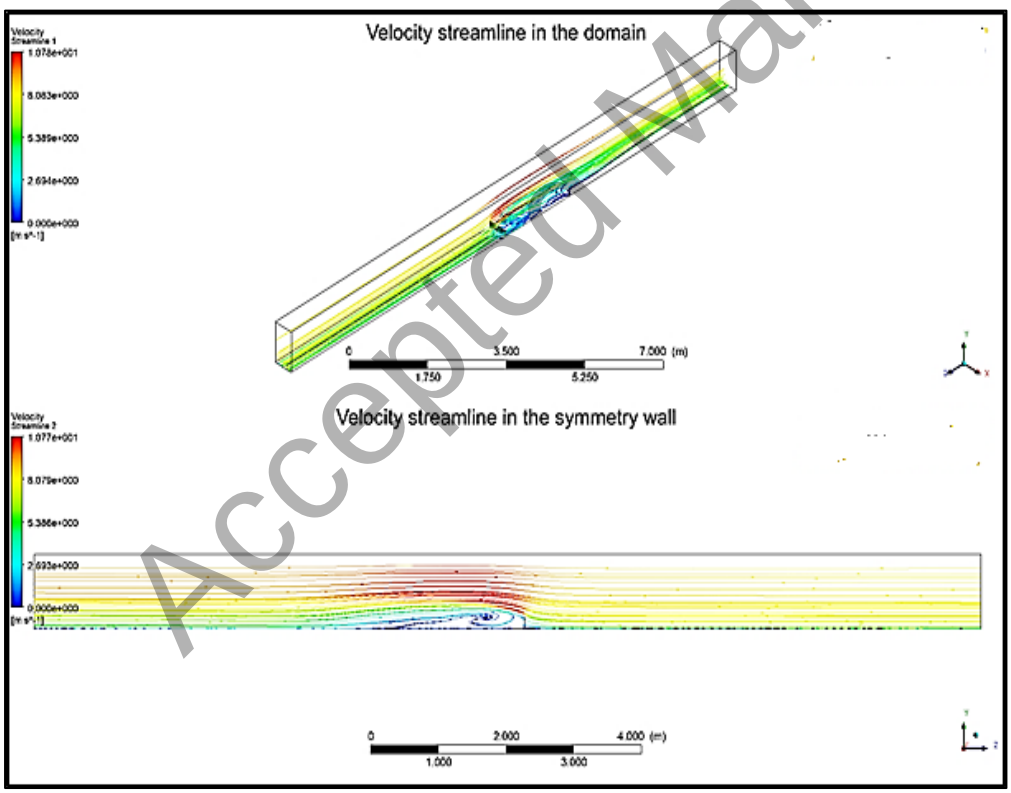


**Figure 11: The velocity streamlines within the entire domain by 3D modelling**

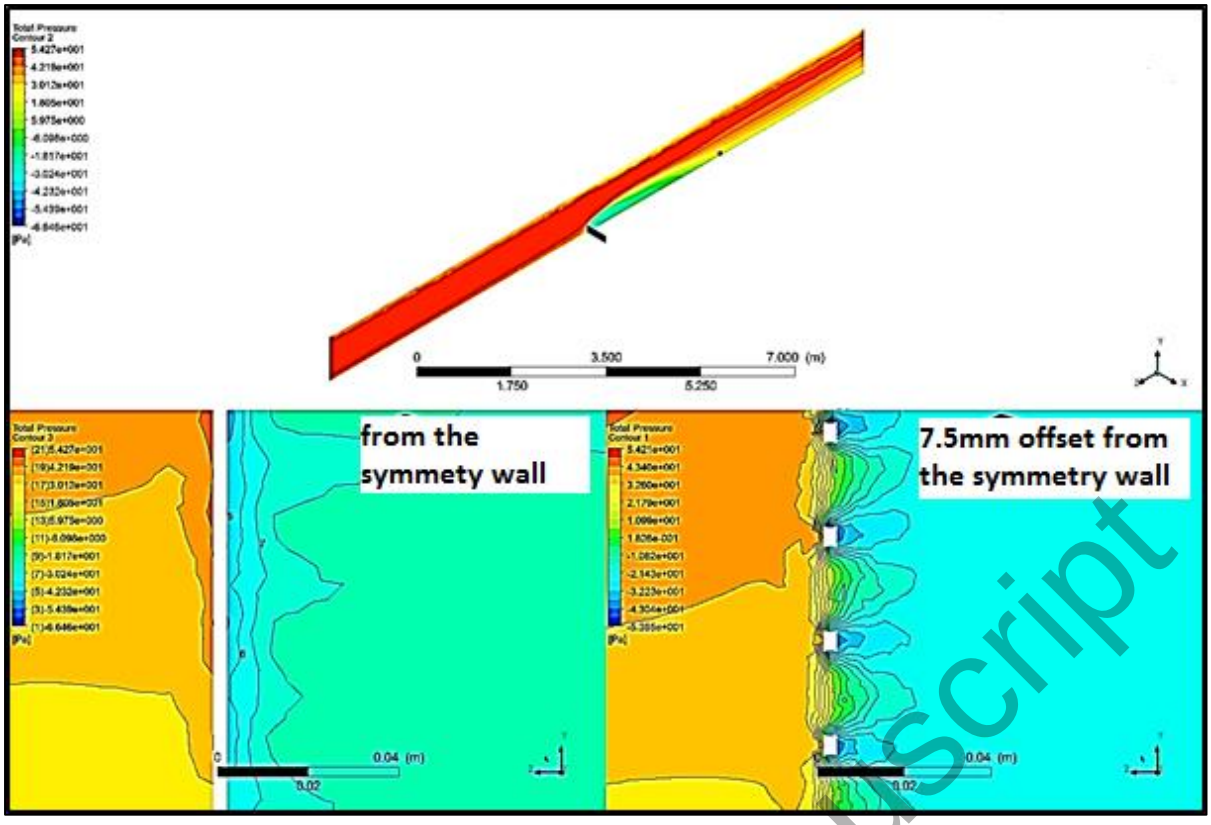


**Figure 12: Contours of total pressure in the planes by 3D modelling**

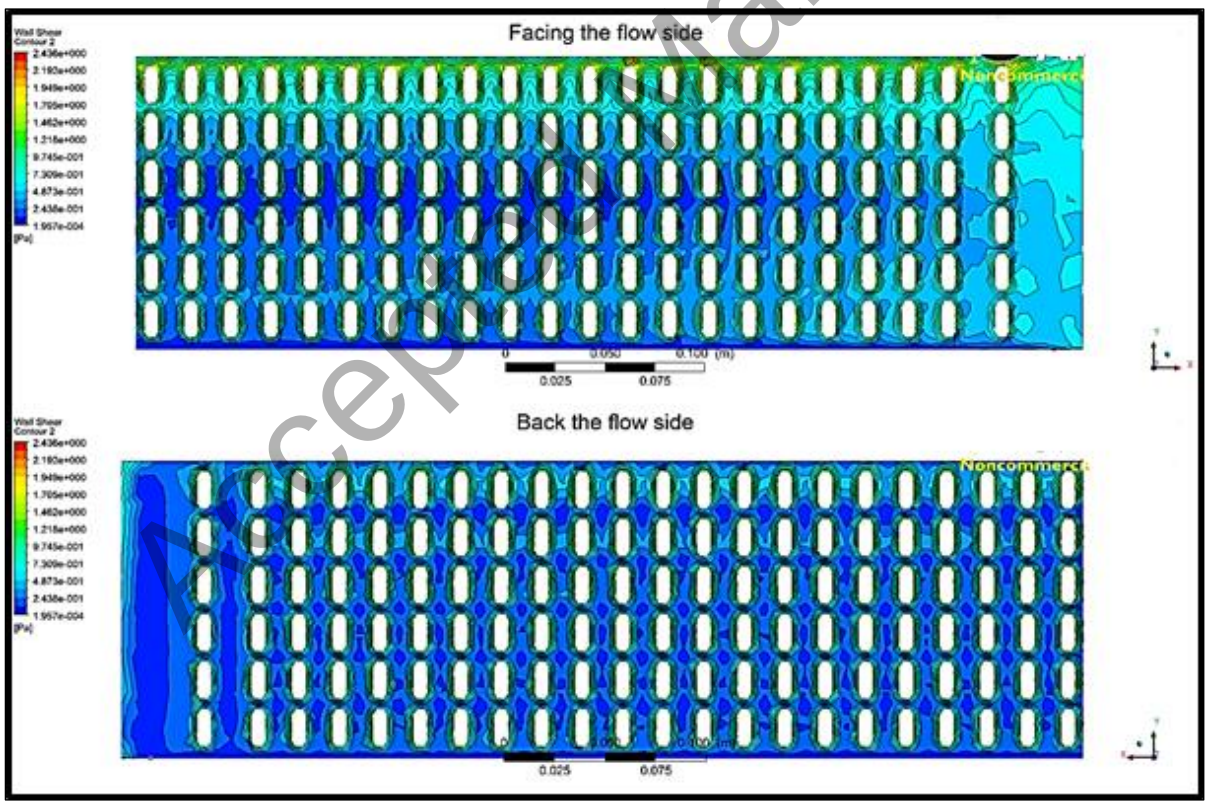


**Figure 13: Contours of wall shear in the fence surface**

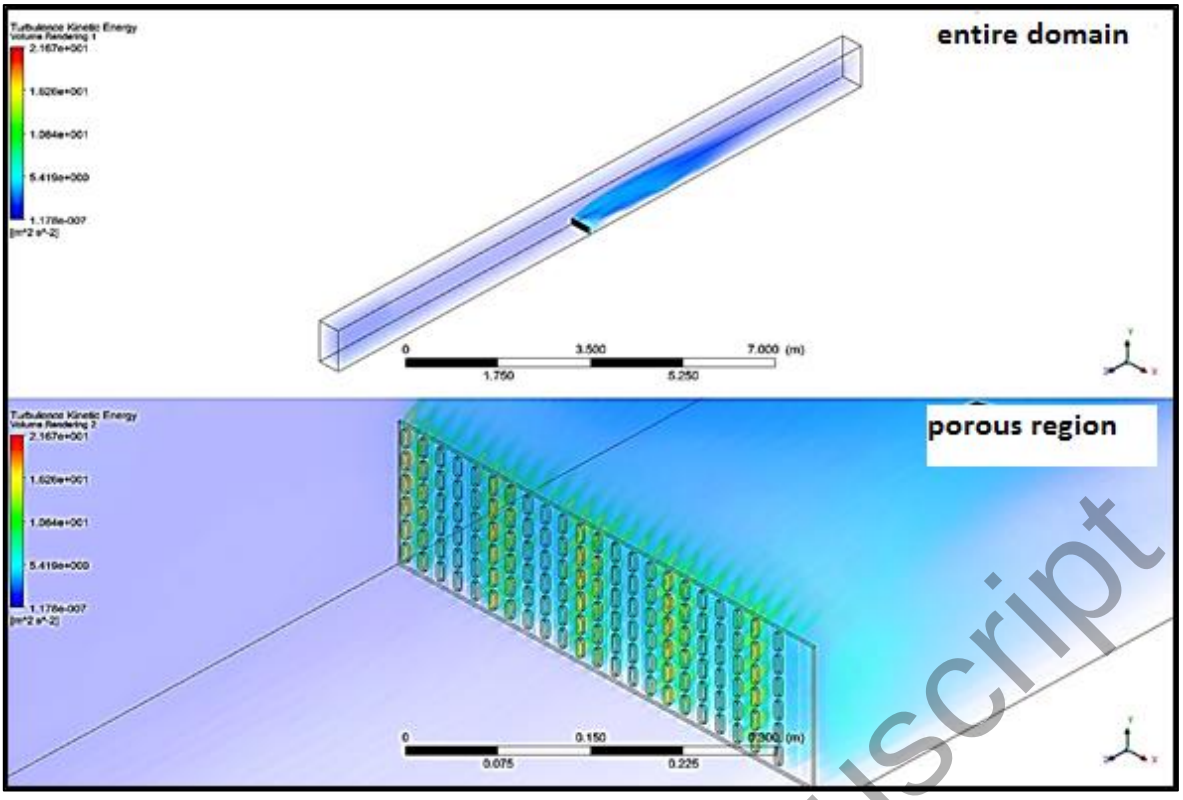


**Figure 14: Volume render of turbulent kinetic energy in the domain**

**Notes on Contributors**

**Yizhong Xu** received his PhD degree in Mechanical Engineering from University of Hertfordshire, UK. His research work covers a wide range of the topics related to civil engineering, composite materials, environmental technology and fluid dynamics. He has expertise in wind tunnel experiments and numerical simulations. He has published about 20 peer-reviewed journal papers and international conference proceedings. At present his is a researcher at Department of Building, Energy and Material Technology at UiT/ the Arctic University of Norway, and is a member of the department research group (BEaM).

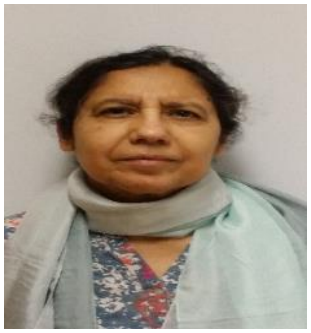

**Rajnish K. Calay** has a broad engineering background with Bachelors in Civil Engineering, India and masters and PhD in Mechanical Engineering from Cranfield University, UK. She has 30 years of experience in academia and industry in UK and India. At present, she is professor in Energy Systems and research leader at the Department of Building, Energy and Material Technology at the Arctic University of Norway, UiT. Her research has a strong focus on investigating thermofluid problems related to buildings, automotive and aerospace applications and providing solutions for better energy efficiency and developing sustainable energy technologies. She has published about 100 peer-reviewed journal publications and international conference papers. Her research outputs cover essential topics related to sustainable built environment (energy saving, thermal comfort and heat transfer), HVAC flows, renewable energy technologies (such as wind energy, bio energy, fuel cell modelling and design). She is a member of Accreditation panel of and Energy Institute, UK, committee member BSI, UK, Editorial Board Member.


**Mohamad Y. Mustafa** is Professor at the Arctic University of Norway, UiT. He has Masters and PhD degrees in Mechanical Engineering from the University of Hertfordshire and Coventry University, UK. He has about 20 years of academic and research experience. His research interests are in sustainable energy, energy efficiency in buildings and HVAC applications. His research work resulted in over 70 scientific publications within different international journals and conferences. He has good research collaboration with industry and educational organizations in Norway and with various institutions outside Norway especially in UK, Finland and China where he is a visiting professor at the School of Mechanical Engineering at Zhejiang University of Technology, Hangzhou, China.